

1 The impact of gaseous degradation on the ~~equilibrium state of gas/particle~~
2 partitioning of methylated polycyclic aromatic hydrocarbons ~~semi-volatile organic~~
3 ~~compounds~~

4 Fu-Jie Zhu^{a,b,c}, Zi-Feng Zhang^{a,b}, Li-Yan Liu^{a,b}, Pu-Fei Yang^{a,b}, Peng-Tuan Hu^{a,d},
5 Geng-Bo Ren^c, Meng Qin^{a,b}, Wan-Li Ma^{a,b,*}

6 ^a International Joint Research Center for Persistent Toxic Substances (IJRC-PTS), State
7 Key Laboratory of Urban Water Resource and Environment, Harbin Institute of
8 Technology, Harbin 150090, China

9 ^b Heilongjiang Provincial Key Laboratory of Polar Environment and Ecosystem
10 (HPKL-PEE), Harbin 150090, China

11 ^c School of Energy and Environmental Engineering, Hebei University of Technology,
12 Tianjin 300401, China

13 ^d School of Environment, Key Laboratory for Yellow River and Huai River Water
14 Environment and Pollution Control, Ministry of Education, Henan Normal University,
15 Xinxiang 453007, China

*Corresponding author. International Joint Research Center for Persistent Toxic Substances (IJRC-PTS), State Key Laboratory of Urban Water Resource and Environment, Harbin Institute of Technology, 73 Huanghe Road, Nangang District, Harbin 150090, Heilongjiang, China.
Email address: mawanli002@163.com

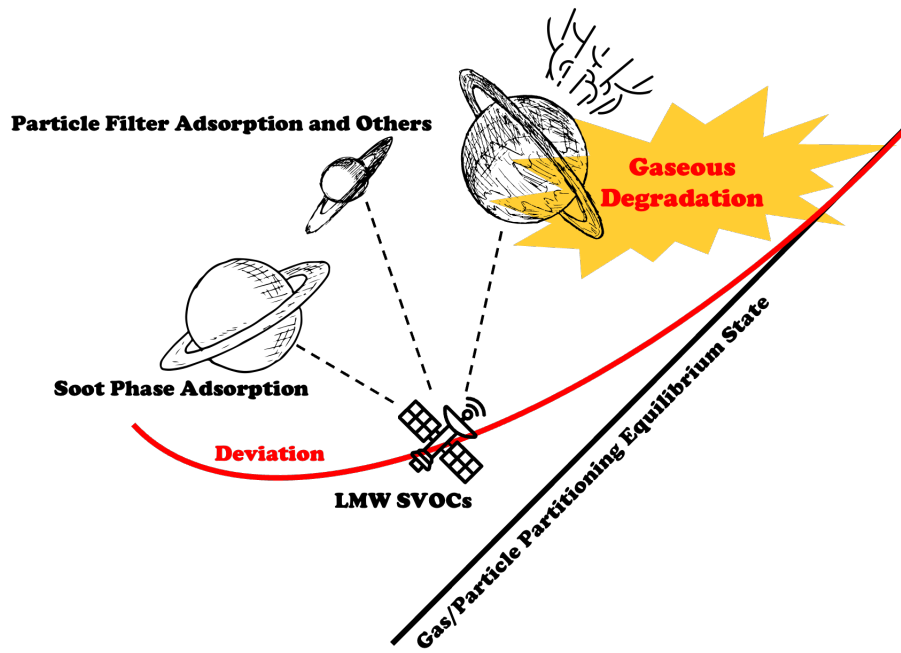
16 **Abstract**

17 The partitioning of semi-volatile organic compounds (SVOCs) between gas and particle
18 phases plays a crucial role in their long-range transport and health risk assessment.
19 However, the accurate predicting of the gas-/particle (~~G/P~~G-P) partitioning quotient
20 (K_P') remains a challenge, especially for the light molecular weight (LMW) SVOCs due
21 to their upward deviation from the equilibrium state. In this study, the phenomenon
22 with the influence of gaseous degradation on G-P partitioning was observed. etie
23 ~~aromatic hydrocarbons (Me-PAHs), it was found that the diurnal variations of~~
24 ~~methylated naphthalenes (Me-Naps, one type of LMW SVOCs) were different from~~
25 ~~other Me-PAHs, that. Specifically, Based on the diurnal study of concentrations and K_P'~~
26 values for methylated polycyclic aromatic hydrocarbons (Me-PAHs), it was found that
27 the K_P' values of methylated naphthalenes (Me-Naps, one type of LMW SVOCs)Me-
28 Naps during daytime were higher than that during nighttime, and the regression lines
29 of $\log K_P'$ versus $\log K_{OA}$ (octanol-air partitioning coefficient) for daytime and
30 nighttime were non-overlap, which were different with other Me-PAHs. It was found
31 ~~that~~Compared with other diurnal influencing factors, the higher gaseous degradation of
32 Me-Naps during in the daytime than that during in the -nighttime should be responsible
33 for partially explain their special diurnal variation of K_P' , which provided a new
34 ~~explanation~~ explanation information for the non-equilibrium behavior of K_P' of LMW
35 SVOCs. Moreover, the influence of gaseous degradation on the deviation of K_P' from
36 the equilibrium state was deeply studied based on athe new steady-state steady-state G-
37 P partitioning G/P partitioning model that theoretical model considering particulate
38 proportion in emission (ϕ_0). The increasing times of K_P' influenced by the gaseous
39 degradation deviated from the equilibrium state can be calculated by $1 + 13.2\phi_0 \times k_{deg}$
40 (gaseous degradation rate). The increasine K_P' increase along with the increasing of k_{deg}

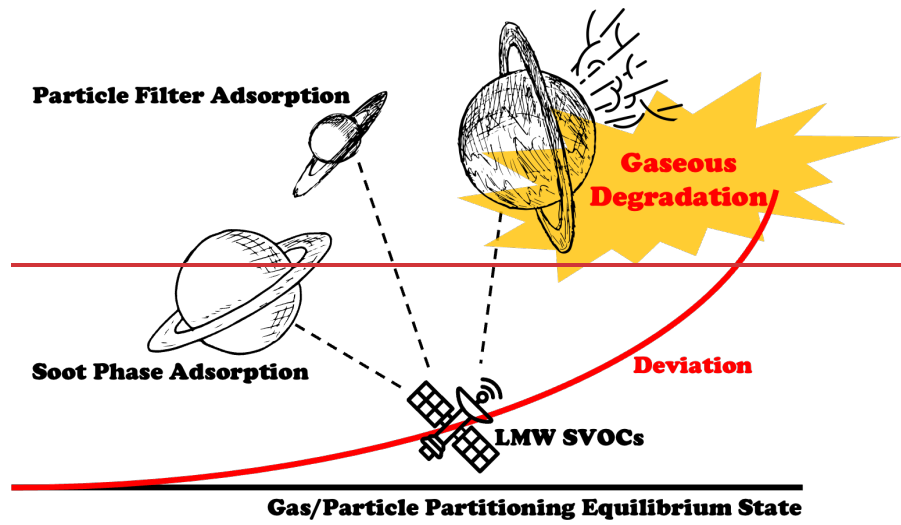
41 ~~proved that higher gaseous degradation in the daytime could increase K_P' value. It was~~
42 ~~found that the deviation occurred when $\phi_0 F_{GR}$ (F_{GR} , degradation flux of gas phase)~~
43 ~~cannot be ignored when compared with F_{GP} (flux from gas phase to particle phase). It~~
44 ~~can be concluded that the deviation was not only related to the gaseous degradation rate~~
45 ~~(k_{deg}), but also related to ϕ_0 . Furthermore, an amplification of K_P' ranging from 1.10 to~~
46 ~~8.45.58 times (90% confidence interval: 1.01 to 14.4) under different ϕ_0 (0 to 1) in the~~
47 ~~temperature range of -50 to 50°C was estimated based on the individual degradation~~
48 ~~rates of Me-Naps and three LMW PAHs estimated by the Monte Carlo aAnalysis. In~~
49 summary, it can be concluded that the influence of gaseous degradation should also be
50 considered for the ~~G/P~~G-P partitioning models of SVOCs, especially for the LMW
51 SVOCs, which provided new insights into the related fields.

52

53 **Keywords:** Equilibrium state; Upward deviation; Light molecular weight SVOCs;
54 Diurnal variation; Methylated polycyclic aromatic hydrocarbons



56



57

58

59 1. Introduction

60 The partitioning of semi-volatile organic compounds (SVOCs) between gas and
61 particle phases, known as gas-/particle (G/P) partitioning, is a crucial process for their
62 long-range atmospheric transport (Li et al., 2020; Zhu et al., 2021b) and their entry
63 pathway into the human body (Hu et al., 2021). To investigate the G/P - G/P partitioning
64 mechanism of SVOCs, researchers have widely employed the correlation between the
65 G/P - G/P partitioning coefficient (K_P) at equilibrium state and the octanol-air partition
66 coefficient (K_{OA}) (Ma et al., 2019; Harner and Bidleman, 1998). The prediction of K_P
67 based on K_{OA} was conducted in previous studies, which deduced some G/P - G/P
68 partitioning models (Qiao et al., 2020). The Harner-Bidleman (H-B) model (Harner and
69 Bidleman, 1998) and the Dachs-Eisenreich (D-E) model (Dachs and Eisenreich, 2000)
70 were successfully applied in the prediction of K_P for different SVOCs using the
71 equilibrium-state theory (Wang et al., 2011; Sadiki and Poissant, 2008). In addition, the
72 Li-Ma-Yang (L-M-Y) model (Li et al., 2015) was ~~established~~ derived based on the
73 steady-state theory, which exhibited good performance for predicting the G/P - G/P
74 partitioning quotient (K_P') at steady state, particularly for high molecular weight (HMW)
75 SVOCs (Qiao et al., 2020; Li et al., 2017; Hu et al., 2020).

76 Previous studies had found that the K_P' deviated from the equilibrium state for both
77 HMW SVOCs (i.e., high $\log K_{OA}$ value) (Li et al., 2015; Li and Jia, 2014) and light
78 molecular weight (LMW) SVOCs ~~(i.e., low $\log K_{OA}$ value)~~ (Ma et al., 2020; Dachs and
79 Eisenreich, 2000). For the HMW SVOCs, the particulate SVOCs were either deposited
80 or removed through dry and wet depositions of particles before reaching equilibrium
81 state, as demonstrated by both the theoretical study (L-M-Y model) and the monitoring
82 study (Mackay et al., 2019; Li et al., 2015), which can be used to explain the deviation.
83 For the LMW SVOCs, ~~in general,~~ the K_P' deviated upward from the equilibrium state,

84 ~~that~~ and the deviation could be multiple orders of magnitude, such as LMW polycyclic
85 aromatic hydrocarbons (PAHs) (Ma et al., 2020; Ma et al., 2019). Several explanations
86 have been proposed for this deviation. First, the artifacts resulting from the adsorption
87 of gaseous PAHs onto particle filters during atmospheric sampling can increase K_p'
88 values (Zhang and McMurry, 1991; Hart et al., 1992; Hart and Pankow, 1994). In an
89 early study, the double filters sampling method demonstrated that gas adsorption onto
90 filters would cause an overestimation of K_p' by a factor of 1.2 to 1.6 times (Hart and
91 Pankow, 1994). However, the overestimation is much lower than the deviation
92 ~~observed in the monitoring data~~ with multiple orders of magnitude. Second, the
93 enhanced adsorption of gaseous SVOCs onto various phases (e.g., soot phase and
94 inorganic phases) within particles has been extensively documented (Shahpoury et al.,
95 2016; Dachs and Eisenreich, 2000). Some G/PG-P partitioning models were
96 established with the consideration of the enhanced adsorption, such as the D-E model
97 and the poly-parameter linear free energy relationships (pp-LFER) model (Shahpoury
98 et al., 2016; Dachs and Eisenreich, 2000). However, these models ~~still~~ cannot fully
99 explain the deviation from the equilibrium state for the LMW SVOCs, such as some
100 LMW PAHs (acenaphthylene (Acy), acenaphthene (Ace), and fluorene (Flu)) (Ma et
101 al., 2020).

102 A recent study delved into the non-equilibrium interplay of G/PG-P partitioning
103 resulting from chemical reactions of SVOCs (Wilson et al., 2020). The study found that
104 when the chemical loss of SVOCs in the gas or particle phase exceeded the
105 replenishment from the particle or gas phase, the K_p' values could deviate from the
106 equilibrium state (Wilson et al., 2020). According to the findings, the upward deviation
107 of LMW SVOCs from the equilibrium state might be caused by the faster chemical loss
108 of SVOCs in the gas phase than the replenishment from the particle phase. However,

109 further studies are required to confirm this hypothesis. Our previous study provided
110 new insights into the deviation from the equilibrium state for several LMW PAHs by
111 studying the diurnal variation of K_p' values (Zhu et al., 2022). The study found that the
112 K_p' values for the three LMW PAHs (Acy, Ace, and Flu) were higher in the daytime
113 than those in the nighttime (Zhu et al., 2022). In addition, the chemical reactions of
114 SVOCs were different between the daytime and nighttime (Ohura et al., 2013).
115 Therefore, the study on the diurnal variation of G/P_G-P partitioning between the
116 daytime and nighttime can be considered as a special case for deep understanding the
117 deviation of LMW SVOCs from the equilibrium state.

118 In order to comprehensively investigate the deviation of the K_p' value from the
119 equilibrium state for LMW SVOCs, the diurnal variation of concentrations and K_p'
120 values for methylated PAHs (Me-PAHs) was conducted in this study. Furthermore, the
121 influence of the gaseous degradation on the deviation of K_p' from the equilibrium state
122 was quantified based on the theoretical model for both LMW Me-PAHs and PAHs,
123 which provided new insights into the G/P_G-P partitioning of SVOCs.

124

125 **2. Materials and methods**

126 **2.1. Sampling method**

127 The detailed information for the sampling method and site can be found in our
128 previous study (Zhu et al., 2022; Zhu et al., 2021a). In brief, the sampling program was
129 conducted at an urban location on the rooftop of a 14-meter-high building in Harbin
130 City in northeastern China. Harbin City has an obvious seasonal variation, with the
131 heating season from 20th October to 20th April and the non-heating season from 20th
132 April to 20th October. A total of 32 pairs of air samples during daytime (9:00 a.m. to
133 5:00 p.m.) and nighttime (9:00 p.m. to 5:00 a.m.) were collected every 10 days from

134 December 2017 to November 2018, which minimized the impact of heavy traffic. The
135 glass fiber filters (GFFs) and polyurethane foam plugs (PUFs) were used to collect
136 particulate and gaseous samples, respectively, using a high-volume air sampler (TE-
137 1000, Tisch Environmental, Ohio, USA) with an air flow rate of 0.24 std m³/min. The
138 GFFs and PUFs were carefully sealed and stored in a refrigerator at -20°C prior to
139 treatment.

140 **2.2. Analysis procedure of Me-PAHs**

141 The analysis procedure for Me-PAHs was identical to that of PAHs (Zhu et al.,
142 2022; Zhu et al., 2021a). In brief, the Soxhlet extraction and active silica gel column
143 were used to extract and purify the GFFs and PUFs samples. Prior to extraction, four
144 surrogates (naphthalene-D8, fluorene-D10, pyrene-D10, and perylene-D12) were
145 added to all samples. The extractions were then solvent-exchanged into isooctane,
146 concentrated to 1 mL in GC vials with 200 ng quantitation standard (phenanthrene-
147 D10). A total of 49 Me-PAHs were analyzed by an Agilent 7890B gas chromatograph
148 coupled with an Agilent 5977 mass spectrometer detector, with the electron-impact
149 ionization and selected ion monitoring mode. Chromatographic resolution was
150 achieved with a DB-5 MS capillary chromatographic column (60 m × 0.25 mm i.d. ×
151 0.25 µm film thickness, J&W Scientific). Ultrapure helium gas (>99.9999%) was used
152 as the carrier gas at a constant flow rate of 1 mL/min. An aliquot (2 µL) of the sample
153 was injected into the multi-mode inlet of the GC/MS at 280°C via the pulsed splitless
154 mode. The column-oven temperature program was as follows: hold at 100°C for 1 min,
155 ramp to 200°C at 40°C /min, hold for 13 min, ramp to 300°C at 80°C /min, hold for 22
156 min, ramp to 310°C at 50°C /min, hold for 11 min with the post run of 310°C, hold for
157 3 min. The transfer line temperature was maintained at 280 °C . For the mass

158 spectrometer, the MS source and quadrupole temperatures were set at 230°C and 150°C,
159 respectively. Detailed information and mass spectrometry parameters for the 49 Me-
160 PAHs are summarized in **Table S1, supporting information (SI)**. A representative
161 chromatogram is depicted in **Fig. S1, SI**.

162 **2.3. Quality assurance/quality control**

163 In order to minimize the errors, rigorous quality assurance/quality control
164 procedures were implemented in the present study. Prior to sampling, GFFs were
165 subjected to a cleaning process involving baking at 450°C for 6 hours, while PUFs were
166 extracted via Soxhlet extraction using dichloromethane for 24 hours and hexane for an
167 additional 24 hours. All glassware utilized in the experimental process was cleaned with
168 dichloromethane and hexane prior to use. Field blanks were conducted on a monthly
169 basis, and laboratory blanks were added for every 11 samples. The quantitation standard
170 was utilized to correct fluctuations of the corresponding instrument signal. The average
171 recoveries of the four surrogates ranged from 70% to 110% for all samples, which were
172 deemed acceptable for the utilization of concentration data without correction via
173 surrogate recoveries. The instrument detection limit (IDL) was calculated as three times
174 of the signal to noise, with IDLs for all Me-PAHs ranging from 0.0154 ng to 0.951 ng
175 (**Table S1, SI**), utilizing a constant injection volume of 2 µL. Concentrations below
176 IDLs were excluded from further calculations. The recoveries of all Me-PAHs with
177 spiked blank samples ranged from 94% to 107%. The final reported concentrations
178 were corrected by the blanks, but not corrected with recoveries of spiked blank samples
179 and surrogates. A five-point calibration curve was established using concentrations of
180 5, 10, 50, 100, and 500 ng/mL, with a correlation coefficient (r^2) exceeding 0.99.

181 **2.4. G/PG-P partitioning quotient**

182 The K_P' ($\text{m}^3/\mu\text{g}$) was calculated based on the following equation:

183
$$K_P' = C_P / (C_G \times TSP) \quad (1)$$

184 where, C_P and C_G are the concentrations (ng/m^3) of Me-PAHs in the particle phase and
185 gas phase, respectively; and TSP is the concentration of the total suspended particles in
186 air ($\mu\text{g}/\text{m}^3$).

187 In general, the value of $\log K_{OA}$ can be calculated using the following equation:

188
$$\log K_{OA} = A + B/T \quad (2)$$

189 where, T is the ambient temperature (K); A and B are constants.

190 For most Me-PAHs, the values of A and B were estimated through the utilization
191 of the pp-LFER equation, which relied on the solute descriptors obtained from the UFZ-
192 LSER database (Baskaran et al., 2021; Ulrich et al., 2017). The calculation methods
193 and corresponding parameters have been concisely summarized in **Tables S2 and S3,**
194 **SI.** By utilizing the values of A and B , the value of K_{OA} for Me-PAHs can be obtained
195 by Eq. (2) at any temperature.

196 **2.5. Data analysis method**

197 The statistical analysis was conducted using the SPSS Software (Version 24.0).
198 Prior to analysis, the normal distribution test was performed via the One-Sample
199 Kolmogorov-Smirnov Test. The Paired Sample t-test was utilized for difference
200 analysis in datasets exhibiting normal distribution, while the Wilcoxon Signed Rank
201 Test was employed for the non-normal distribution datasets. Results were considered
202 as statistically significant if the p -value was less than 0.05.

203

204 **3. Results and discussion**

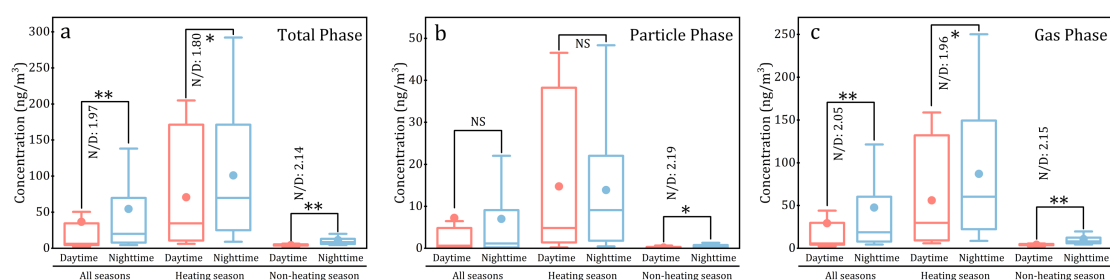
205 **3.1. Diurnal variation of concentration**

206 Among the 49 Me-PAHs, 30 Me-PAHs were frequently detected with detection
207 rates exceeding 30% (**Table S1, SI**), whichand they were considered for further

208 discussion. As depicted in **Fig. 1a**, the total concentrations of 30 Me-PAHs (Σ Me-PAHs)
209 in total phase (particle phase + gas phase) were compared between daytime and
210 nighttime in different seasons. A clear diurnal variation with higher concentrations of
211 Me-PAHs during nighttime as compared to daytime was observed. The geometric mean
212 (GM) concentrations (range of 25th% to 75th%) of Σ Me-PAHs were 12.0 ng/m³ (4.51
213 to 34.6 ng/m³) and 23.6 ng/m³ (7.97 to 69.9 ng/m³) in daytime and nighttime,
214 respectively. ~~These concentrations were comparable with those in air of urban (mean,~~
215 ~~29.8 ng/m³) and semi-urban areas (mean, 23.0 ng/m³) in Toronto City, Canada (Moradi~~
216 ~~et al., 2022).~~ Furthermore, the concentrations of Σ Me-PAHs in total phase during
217 nighttime were significantly higher than those during daytime ($p < 0.05$), with the GM
218 value of nighttime/daytime (N/D) ratios of 1.97 for the whole sampling period.
219 Although studies on the diurnal variation of Me-PAHs are limited, similar diurnal
220 variations have also been observed in some previous studies for other PAHs, such as
221 PAHs, chlorinated-PAHs, ~~nitrate~~~~nitro~~-PAHs, and ~~oxygenated~~~~oxy~~-PAHs (Cao et al.,
222 2018; Ohura et al., 2013; Zhang et al., 2018; Zhu et al., 2022). It was found that the
223 diurnal variations of emission sources, emission intensity, atmospheric reactions, and
224 meteorological effects were responsible for the diurnal variation of SVOCs
225 concentrations (Ohura et al., 2013; Zhang et al., 2018).

226 Moreover, it is noteworthy that distinctly diurnal variations were observed among
227 different phases (gas and particle) and different seasons (heating and non-heating) (**Fig.**
228 **1b and Fig. 1c**). Notably, a significant increase of ~~nighttime~~ concentrations during
229 nighttime compared to that during daytime was observed for the gas phase ($p < 0.01$),
230 while no significant diurnal variation was observed for the particle phase in all seasons
231 and in heating season. Additionally, the N/D ratios were higher in the non-heating
232 season compared to the heating season. For instance, in the non-heating season, the GM

233 N/D ratios were 2.14 and 2.15 for the total and gas phases, respectively. However, in
 234 the heating season, the GM N/D ratios were 1.80 and 1.96 for the total and gas phases,
 235 respectively. These findings suggested that gaseous Me-PAHs exhibited more
 236 obviously diurnal variation than particulate Me-PAHs, and Me-PAHs in the non-
 237 heating season displayed more prominent diurnal variation than that in the heating
 238 season.



239

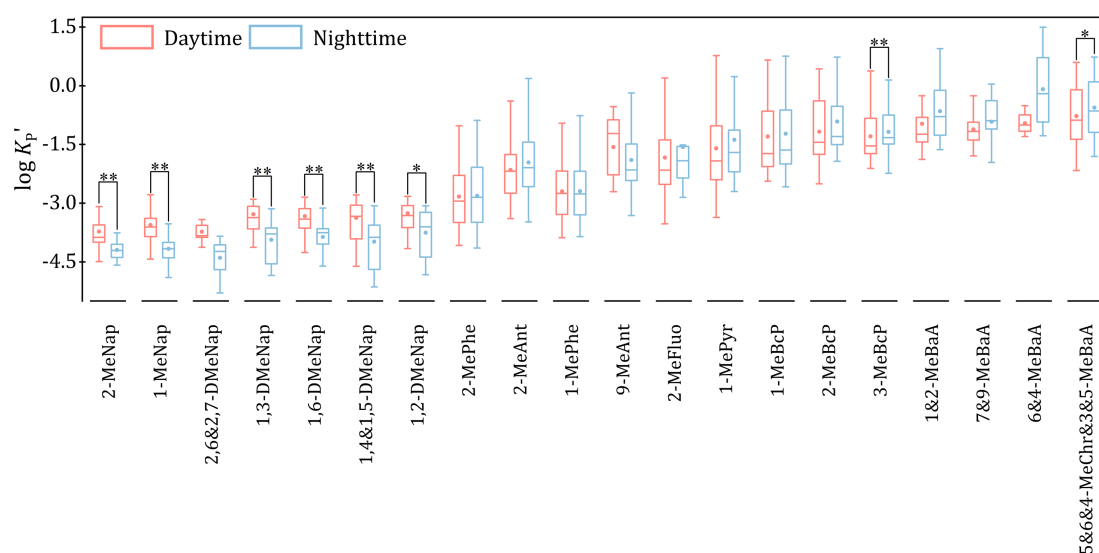
240 **Fig. 1.** Comparison with the concentrations of the ΣMe-PAHs between daytime and nighttime in
 241 different seasons for different phases (Note: * and ** represent that the differences are significant
 242 at 0.05 level and 0.01 level, respectively; NS represents no significant difference; N/D represents
 243 the geometric mean value of nighttime/daytime ratio for concentration.)

244 Furthermore, it is interesting to note that individual Me-PAHs also exhibited
 245 different diurnal variations. The N/D ratios, and the GM values of N/D ratios for
 246 individual Me-PAHs are presented in **Table S4 and Fig. S2, SI**. The GM values of N/D
 247 ratios varied considerably among different Me-PAHs, ranging from 0.347 to 7.30.
 248 Regarding to the seasonal differences in diurnal variation (**Table S4, SI**), the results for
 249 most individual Me-PAHs were consistent with those for ΣMe-PAHs, with higher GM
 250 values of N/D ratios in the non-heating season than the heating season. With respect to
 251 the phase differences in diurnal variation (**Table S4 and Fig. S2, SI**), the GM values of
 252 N/D ratios in the gas phase for Me-naphthalenes (Me-Naps, one type of LMW SVOCs)
 253 were significantly higher than those in the particle phase for individual Me-Naps in all
 254 seasons. This result with Me-Naps was consistent with that of ΣMe-PAHs, which could
 255 be attributed to the high contribution of Me-Naps to ΣMe-PAHs (mean value: 63%).

256 However, for other Me-PAHs (Table S4 and Fig. S2, SI), the N/D ratios in the particle
257 phase were similar or even a little higher than those in the gas phase.

258 3.2. Diurnal variation of G/P-P partitioning

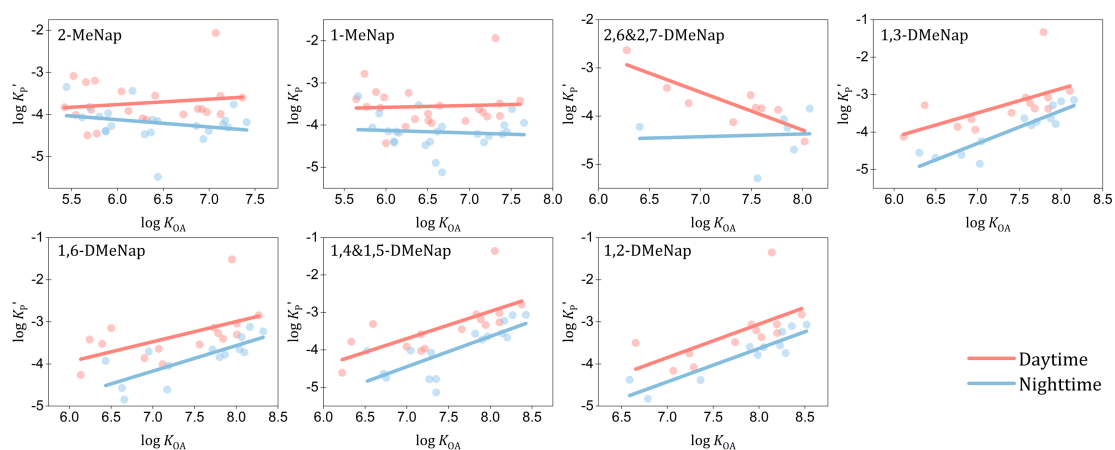
259 In general, the different diurnal variations with the concentrations of SVOCs
260 between the gas phase and particle phase could cause the diurnal variations of K_P' values.
261 As depicted in Fig. 2, compared with other Me-PAHs, several LMW Me-PAHs (such
262 as Me-Naps) exhibited significantly higher $\log K_P'$ values in the daytime compared to
263 the nighttime ($p < 0.05$). However, the other Me-PAHs, like 3-MeBcP, 5&6&4-MeChr,
264 and 3&5-MeBaA, had higher $\log K_P'$ values in the nighttime than those in the daytime
265 ($p < 0.05$). The special diurnal variations of the $\log K_P'$ of ~~these~~ Me-Naps can be
266 attributed to the different diurnal variations of their concentrations between the two
267 phases. For example, the N/D ratios of concentrations in the gas phase were
268 significantly higher than those in the particle phase for Me-Naps, which was different
269 from other Me-PAHs (Fig. S2, SI).



270

271 Fig. 2. Comparison of the values of $\log K_P'$ for individual Me-PAHs between daytime and
272 nighttime (Note: * and ** represent that the differences are significant at 0.05 and 0.01 level,
273 respectively.)

274 In order to deeply investigate the diurnal variations of $G/PG-P$ partitioning
 275 quotient, the regression lines of $\log K_P'$ against $\log K_{OA}$ were compared between
 276 daytime and nighttime. In general, the diurnal variations were also observed for the
 277 relationships between $\log K_P'$ and $\log K_{OA}$ for Me-Naps. Interestingly, for these Me-
 278 Naps, the regression lines also had obvious diurnal variations as being higher during
 279 daytime compared to nighttime (Fig. 3). In contrast, no significant differences were
 280 observed in the regression lines for the total Me-PAHs (Fig. S3, SI) and other individual
 281 Me-PAHs (Fig. S4, SI) between daytime and nighttime. Given the lower ambient
 282 temperatures during nighttime, higher K_P' values during nighttime compared to daytime
 283 and the overlap of the two regression lines between daytime and nighttime were
 284 expected, just like the total Me-PAHs (Fig. S3, SI) and other individual Me-PAHs (Fig.
 285 S4, SI). However, the different phenomenon with the regression lines of $\log K_P'$ against
 286 $\log K_{OA}$ was observed for Me-Naps (Fig. 3).



287
 288 **Fig. 3.** The regression lines of $\log K_P'$ against $\log K_{OA}$ between daytime and nighttime for Me-
 289 Naps

290 The specific relationships with concentrations between daytime and nighttime K_P'
 291 and concentrations for these Me-Naps can be elucidated by the following equations:

292 ~~_____~~ $C_{P,N}/C_{P,D} < C_{G,N}/C_{G,D} \rightarrow C_{P,N}/C_{G,N} < C_{P,D}/C_{G,D}$ (3)

293 where, ~~N/D_P and N/D_G are the N/D ratios of particle phase and gas phase, respectively;~~

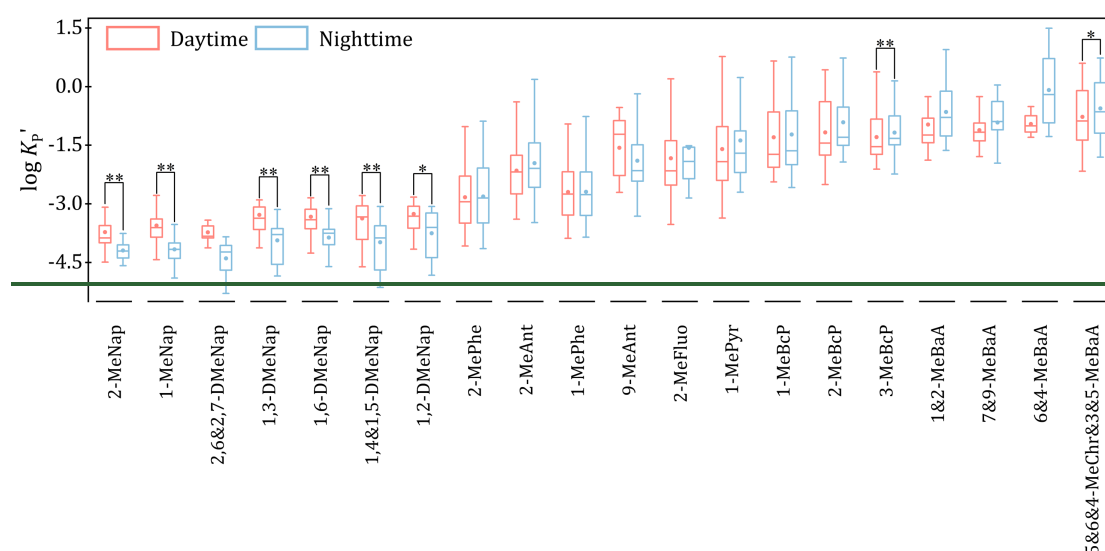
294 $C_{P,N}$ and $C_{P,D}$ are the particulate concentrations during nighttime and daytime,
295 respectively; $C_{G,N}$ and $C_{G,D}$ are the gaseous concentrations during nighttime and
296 daytime, respectively.

297 In addition, no significant difference was observed for *TSP* concentrations
298 between daytime and nighttime (GM: 94.5 $\mu\text{g}/\text{m}^3$ in the daytime and 90.5 $\mu\text{g}/\text{m}^3$ in the
299 nighttime). Therefore, the following relationship can be derived:

300 $C_{P,N}/C_{G,N}/TSP_N < C_{P,D}/C_{G,D}/TSP_D \rightarrow K'_{P,N} < K'_{P,D}$ (54)

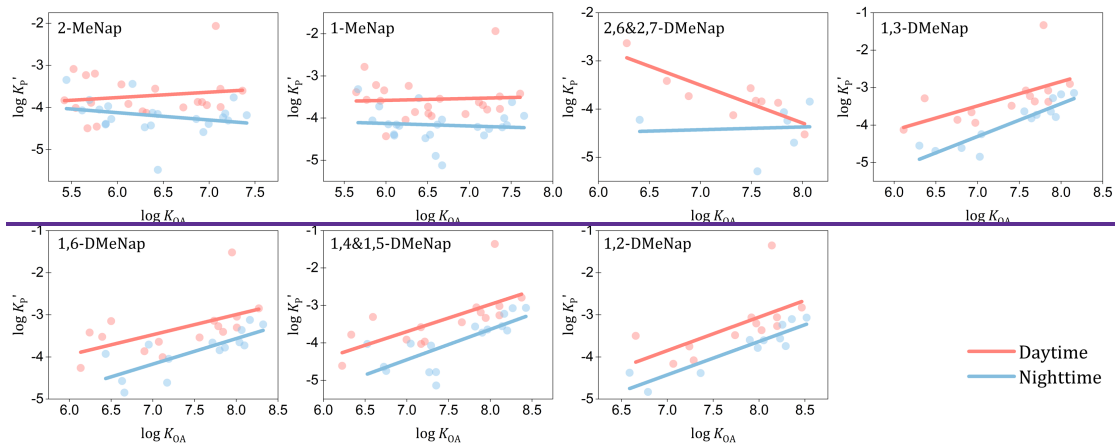
301 where, TSP_N and TSP_D are the *TSP* concentrations during nighttime and daytime,
302 respectively; $K'_{P,N}$ and $K'_{P,D}$ are the K'_P values during nighttime and daytime,
303 respectively.

304 When Eqs. (3), ~~(4)~~, and ~~(54)~~ were considered together, ~~therefore~~, it can be found
305 that the higher N/D ratios of concentrations in the gas phase than those in the particle
306 phase could ~~caused the~~ higher K'_P values during daytime than those during nighttime.
307 Therefore, the higher log K'_P values in the daytime than the nighttime for Me-Naps (Fig.
308 2) can be explained by the findings with the values of N/D ratios between particle phase
309 and gas phase (Fig. S2 in SI). The clarification of the influence factors in the special
310 diurnal variation of the concentrations of these Me-Naps, would help to understand the
311 diurnal variation of G-P partitioning of LMW SVOCs.



~~Fig. 2. Comparison of the values of $\log K_p'$ for individual Me-PAHs between daytime and nighttime (Note: * and ** represent that the differences are significant at 0.05 and 0.01 level, respectively.)~~

~~In order to deeply investigate the diurnal variations of G/P partitioning, the regression lines of $\log K_p'$ against $\log K_{OA}$ were compared between daytime and nighttime. In general, diurnal variations were also observed for the relationships between $\log K_p'$ and $\log K_{OA}$ for Me-Naps. Interestingly, for these Me-Naps, the regression lines also had obvious diurnal variations as being higher during daytime compared to nighttime (Fig. 3). In contrast, no significant differences were observed in the regression lines for the total Me-PAHs (Fig. S3, SI) and other individual Me-PAHs (Fig. S4, SI) between daytime and nighttime. Given the lower ambient temperatures during nighttime, higher K_p' values compared to daytime and the overlap of the two regression lines between daytime and nighttime were expected, just like the total Me-PAHs (Fig. S3, SI) and other individual Me-PAHs (Fig. S4, SI). However, the different phenomenon was observed for Me-Naps (Fig. 3). These findings suggested that the diurnal variations of G/P partitioning for Me-Naps may be also influenced by other environmental parameters beyond ambient temperature.~~



330

331 **Fig. 3.** The regression lines of $\log K_p'$ against $\log K_{OA}$ between daytime and

332 nighttime for Me-Naps. As noted in previous studies, the concentrations of SVOCs are

333 influenced by emission intensity, atmospheric reactions, and meteorological effects

334 (Ohura et al., 2013; Zhang et al., 2018) (Ohura et al., 2013; Zhang et al., 2018). In

335 general, emission intensity can impact the concentration of SVOCs in the total phase

336 (gas phase plus particle phase), while they cannot affect the distribution between the

337 two phases when the steady state has been reached. In other words, this factor cannot

338 cause the diurnal variation of the G/P-G-P partitioning for Me-Naps. Among

339 meteorological parameters, temperature is the key factor on the G/P-G-P partitioning of

340 SVOCs, which could result in the higher K_p' values during nighttime than those during

341 daytime. However, the opposite results were observed for Me-Naps in this study, which

342 suggested the influences of other factors. As mentioned in previous studies, the higher

343 atmospheric reactions in the daytime resulted in the lower concentrations of SVOCs in

344 the daytime than those in the nighttime (Ohura et al., 2013; Reisen and Arey,

345 2005) (Ohura et al., 2013; Reisen and Arey, 2005), which might also be responsible for

346 the special diurnal variations of the K_p' values of Me-Naps. Previous studies also

347 suggested that when the rate of chemical loss is faster than the process of G/P-G-P

348 partitioning (or the degradation in the gas phase exceeded the replenishment from the

349 particle phase), the G/P-G-P partitioning maybe deviate from the equilibrium state

(Wilson et al., 2020)²⁰). In addition, the value of K_p' increased along with the increase of the chemical loss rate (Wilson et al., 2020). Therefore, it can be concluded that the higher gaseous degradation during daytime than that during nighttime might result in higher K_p' values during daytime. The observation of the higher K_p' for these Me-Naps in the daytime than those in the nighttime provided the new insight into the deviation of K_p' from the equilibrium state for LMW SVOCs.

3.3. Influence of gaseous degradation on K_p' of LMW SVOCs

~~3.3. Influence of gaseous degradation on the deviation of LMW SVOCs from equilibrium state~~

~~As noted in previous studies, the diurnal variations of SVOCs concentrations are influenced by emission intensity, atmospheric reactions, and meteorological effects (Ohura et al., 2013; Zhang et al., 2018). In general, emission intensity can impact the concentration of SVOCs in the total phase (gas phase plus particle phase), while they cannot affect the distribution between the two phases when the steady state has been reached. In other words, this factor cannot cause the diurnal variation of the G/P partitioning for Me Naps. Among meteorological parameters, temperature is the key factor on the G/P partitioning of SVOCs, which could result in the higher K_p' values during nighttime than those during daytime. However, the opposite results were observed for Me Naps in this study, which suggested the influences of other factors. Therefore, As mentioned in previous studies, the atmospheric reactions was responsible for the higher concentrations of SVOCs in the time than those in the time (Ohura et al., 2013; Reisen and Arey, 2005), which might also be responsible for the diurnal variations of the K_p' values of Me Naps (Ohura et al., 2013; Reisen and Arey, 2005). Previous studies have also suggested that when the rate of chemical loss is faster than the process of G/P partitioning (or the degradation in the gas phase exceeded the~~

375 replenishment from the particle phase), the G/P partitioning may deviate from the
 376 equilibrium state (Wilson et al., 2020). In addition, the value of K_p' increased along with
 377 the increase of the chemical loss rate (Wilson et al., 2020). Therefore, it can be
 378 concluded that the higher gaseous degradation during daytime than that during
 379 nighttime, might result in the higher K_p' values during daytime than that during
 380 nighttime. In the above section, it was found that the higher gaseous degradation during
 381 daytime than that during nighttime might result in the higher K_p' values during daytime
 382 than that during nighttime. Furthermore ~~Therefore, we can deduce that the gaseous~~
 383 ~~degradation might result in the upward deviation of K_p' from equilibrium state. Here~~
 384 this section, the fugacity model/new steady-state G-P partitioning model (Zhu et al.,
 385 2023) was applied for better understanding the impact of gaseous degradation on the
 386 deviation of K_p' from equilibrium state. Based on the model, for the LMW SVOCs, the
 387 K_p' values can be obtained using the following simplified equation, and more detailed
 388 information about the equation were presented in Text S1, S1:

$$389 \quad \log K_p' = \log K_{p-HB} + \log(f_p/f_g) \quad (65)$$

390 where, K_{p-HB} represents the predicted G/P partitioning coefficient from the H-B model (the
 391 equilibrium state model, $\log K_{p-HB} = \log K_{OA} + \log f_{OM} = 11.91$, f_{OM} is the fraction of the organic
 392 matters in particles) (Harner and Bidleman, 1998); f_p is the fugacity for particle phase; and f_g is the
 393 fugacity for gas phase.

394 According to the Eq. (65), K_p' will upward deviate from K_{p-HB} (or the equilibrium state) when
 395 $f_p > f_g$. Based on our previous study (Zhu et al., 2023), the fugacity ratio of the particle phase to the
 396 gas phase can be expressed as Eq. (76), when the steady state is reached between gas phase and
 397 particle phase:

$$398 \quad \frac{f_p}{f_g} = \frac{D_{GP} + \phi_0 D_{GR}}{D_{GP} + (1 - \phi_0)(D_{PD} + D_{PW})} \quad (76)$$

399 where, ϕ_0 is the particulate proportion of SVOCs in emission; D_{GP} is the intermedia D value
 400 between gas phase and particle phase; D_{GR} is the D value for the degradation of gas phase SVOCs;
 401 D_{PD} and D_{PW} are the D values of the dry and wet depositions of particle phase SVOCs, respectively.

402 For the LMW SVOCs, the dry and wet deposition fluxes of particle phase ($F_{PD} + F_{PW}$) (Fig.
 403 S5, SI) can be ignored, then the Eq. (76) can be expressed as follows:

$$404 \quad \frac{f_P}{f_G} = 1 + \frac{\phi_0 D_{GR}}{D_{GP}} \quad (87)$$

405 Based on the above equation, when $\phi_0 D_{GR}$ cannot be ignored compared with D_{GP} , f_P will be
 406 higher than f_G , and the K_P' values will deviate upward from equilibrium state. In other words, when
 407 $\phi_0 F_{GR}$ ($F_{GR} = f_G D_{GR}$, the degradation flux of gas phase) cannot be ignored compared with F_{GP} (F_{GP}
 408 $= f_G D_{GP}$, the flux from gas phase to particle phase), the K_P' values will deviate upward from
 409 equilibrium state. Therefore, it can be concluded that the deviation was affected by both the gaseous
 410 degradation and the particulate proportion of SVOCs in emission.

411 By simplifying the Eq. (76) and adding to Eq. (56), the new steady-state G/P
 412 partitioning model can be obtained (Zhu et al., 2023):

$$413 \quad \log K'_{P-NS} = \log K_{P-HB} + \log(1 + 13.2\phi_0 \times k_{deg}) \quad (985)$$

414 where, K'_{P-NS} is the predicted G/P_{G-P} partitioning quotient of the new steady-state
 415 G/P_{G-P} partitioning model; K_{P-HB} is the G-P partitioning coefficient calculated from
 416 the H-B model (the equilibrium-state model, $\log K_{P-HB} = \log K_{OA} + \log f_{OM} - 11.91$, f_{OM}
 417 is the organic matters in the particles) (Harner and Bidleman, 1998); ϕ_0 is the particulate
 418 proportion of SVOCs in emission; k_{deg} is the degradation rate of SVOCs in gas phase
 419 (h^{-1}).

420 Based on Eq. (985), the value of K_P' will increase along with the increasing of k_{deg} .
 421 As we mentioned above, the gaseous degradation in the daytime was higher than those
 422 in the nighttime values of K_P' . Therefore, the application of Eq. (5) can demonstrate that

423 the gaseous degradation of Me-Naps could be the part of reason for the higher K_p' in
424 the daytime than that in the nighttime.

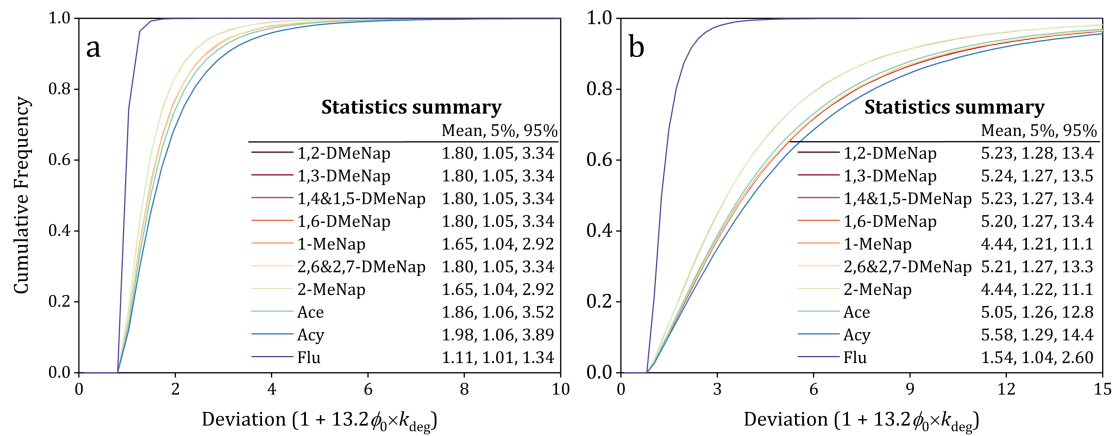
425 ~~The exact the influence of gaseous degradation on G/P partitioning for LMW~~
426 ~~SVOCs can be comprehensively studied by~~Based on the new steady state G/P
427 partitioning model (Eq. (8)). Therefore, it can be concluded that the deviation with K_p'
428 from the equilibrium state for LMW SVOCs can be expressed as $\log(1 + 13.2\phi_0 \times k_{deg})$,
429 ~~which was related to k_{deg} and ϕ_0 .~~The impact from gaseous degradation on G/P
430 partitioning was quantified using the theoretical method (Eq. (9)). Furthermore, the
431 deviation with K_p' from the equilibrium state ($\log K_{P-HB}$) caused by the gaseous
432 degradation for LMW SVOCs can be estimated using the equation of $\log(1 + 13.2\phi_0 \times$
433 $k_{deg})$, which was related to k_{deg} and ϕ_0 . The k_{deg} values under 25°C for the Me-Naps and
434 the three LMW PAHs (Acy, Ace, and Flu) were calculated using their half-lives from
435 the Estimation Programs Interface (EPI) Suite (Table S5, SI). Then, the k_{deg} values
436 under different temperature (-50 ~~to~~ and 50°C) were calculated using the following
437 equation:

$$k_{deg_T} = k_{deg_0} \exp\left(\frac{E_{aA}}{R\left(\frac{1}{T_0} - \frac{1}{T}\right)}\right) \quad (1096)$$

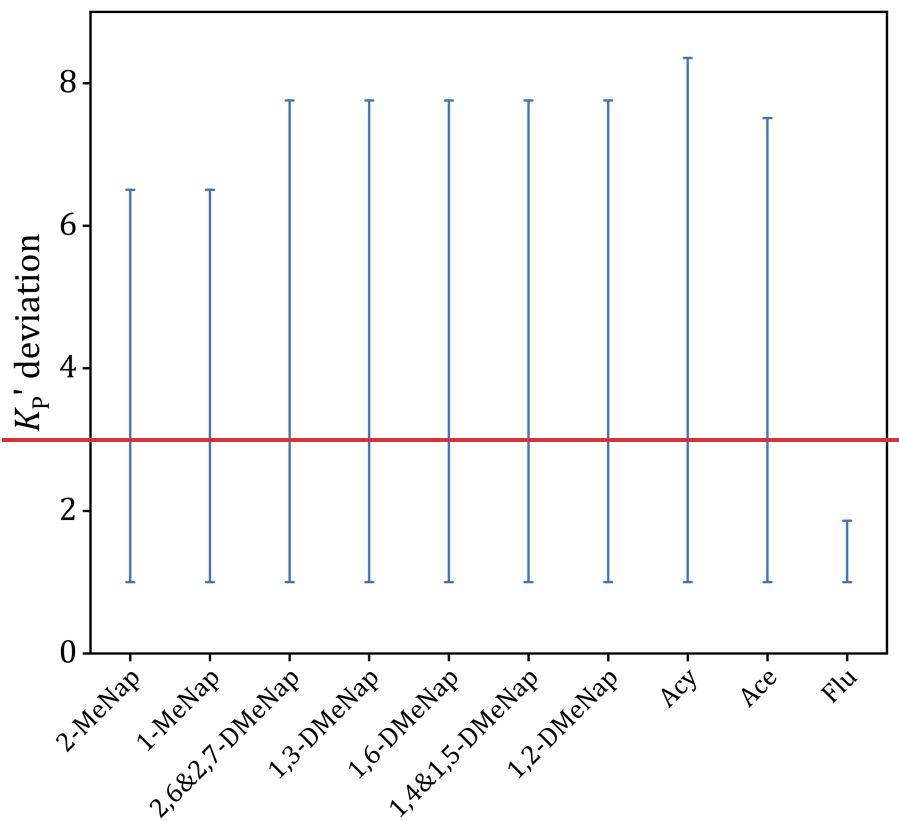
439 where, k_{deg_T} is the k_{deg} value at temperature T ; k_{deg_0} is the k_{deg} value at 25°C; E_{aA} is the
440 activation energy in air (J/mol); R is the universal gas constant (8.314 J·K/mol); T and
441 T_0 (25°C) are temperature (K). The minimum and maximum k_{deg} values for these PAHs
442 under ~~the different~~ temperature ~~range of -50 to 50°C~~ were summarized in Table S5, SI.

443 The increasing times of K_p' values influenced by the gaseous degradation deviated
444 from the equilibrium state can be calculated based on the equation: $1 + 13.2\phi_0 \times k_{deg}$.
445 To evaluate the impact of the gaseous degradation on the K_p' deviated from equilibrium
446 state, the sensitivity analysis at condition of -50°C and 50°C was separately conducted

447 by the Monte Carlo Analysis with 100 000 trials employing the commercial software
448 package Oracle Crystal Ball. Considering the influence of ϕ_0 on the gaseous degradation,
449 the minimum impact of k_{deg} on K_p' deviation occurred when ϕ_0 was set to 0. On the
450 other hand, the maximum impact of k_{deg} on K_p' deviation was observed when ϕ_0 was set
451 to 1. Consequently, the range of the impact resulting from the gaseous degradation was
452 calculated for individual PAHs, and the results are presented in **Fig. 4**. It can be found
453 that, the mean impact caused by the gaseous degradation on K_p' deviation for these
454 PAHs was were in the range of 1.10 to 1.98 times (90% confidence interval: 1.01 to
455 3.89) (**Fig. 4a**) and in the range of 1.54 to 5.58 times (90% confidence interval: 1.04 to
456 14.4) (**Fig. 4b**) at -50°C and 50°C , respectively. The influence from the gaseous
457 degradation on the deviation of K_p' from the equilibrium state could approach to one
458 order of magnitude, which cannot be ignored in the study of G-P partitioning of SVOCs.
459 in the range of 1 to 8.4 times under different ϕ_0 (0 to 1) in the temperature range of -50
460 to 50°C . However, due to the limited consideration of the gaseous degradation (only
461 reaction with hydroxyl radicals) in this study, the actual impact of the gaseous
462 degradation on K_p' deviation was expected to be higher than the range.



463



464

465 **Fig. 4.** The impact of the gaseous degradation on the time of deviation of K_p' deviation from the
 466 equilibrium state calculated-estimated based on the Monte Carlo Analysis at condition of -50°C

467 (a) and 50°C (b). Eq. (9) (Note: The following variables with their distribution patterns and

468 confidence factors (CF) were considered: ϕ_0 : uniform distribution, 0 to 1; k_{deg} , lognormal

469 distribution; CF = 3 (Wania and Dugani, 2003).)

470 4. Implications

471 According to previous studies, adsorption of gaseous SVOCs onto filters during
472 sampling (Hart and Pankow, 1994) and enhanced adsorption of gaseous SVOCs onto
473 various phases (e.g., soot phase) (Dachs and Eisenreich, 2000) both can influence the
474 equilibrium state of G/PG-P partitioning. Additionally, the present study revealed that
475 the gaseous degradation also caused the deviation of K_P' from the equilibrium state.
476 Therefore, in the present study, the deviation of K_P' from the equilibrium state caused
477 by these factors were estimated and compared in order to deeply understand the
478 influence of gaseous degradation. As mentioned in above section, the mean deviation
479 resulting from gaseous degradation was estimated (K_P' : 1.10 to 8.45.58 times increased);
480 ~~with the logarithmic deviation of K_P' in the range of 0 to 0.925~~. The deviation caused
481 by the influence of the soot phase within the particles was estimated by averaging the
482 difference between the predictions of the H-B model (Harner and Bidleman, 1998) and
483 the D-E model (Dachs and Eisenreich, 2000) for LMW SVOCs with the range of log
484 K_{OA} from 5 to 9. The ~~logarithmic deviation increasing times~~ of K_P' caused by the
485 influence of the soot phase within the particles was in the range of 0.4292.68 to
486 0.8877.70 times (~~K_P' : 2.68 to 7.70 times increased~~). A previous study pointed out that
487 the effect of the adsorption of gaseous SVOCs onto filters could ~~cause the logarithmic~~
488 ~~deviation of increase~~ K_P' ~~in a range of about~~ 0.07921.2 to 1.60.204 times (~~K_P' : 1.2 to 1.6~~
489 ~~times increased~~) (Hart and Pankow, 1994). Therefore, it can be found that, the deviation
490 of K_P' from the equilibrium state caused by the gaseous degradation was comparable
491 with that caused by the adsorption of the soot phase, which were both higher than that
492 caused by the adsorption of gaseous SVOCs onto filters. Therefore, it can be concluded
493 that the influence of gaseous degradation should also be considered for the G/PG-P
494 partitioning models of SVOCs, especially for the LMW SVOCs.

495 ~~It is worth noting that the present study only considered the gaseous degradation~~
496 ~~related to the reaction with hydroxyl radicals, however did not consider the gaseous~~
497 ~~degradation routes resulting from other atmospheric oxidation pathways and~~
498 ~~photodegradation were not included, which may lead to an underestimation of the~~
499 ~~impact of the total gaseous degradation. In addition, previous studies have demonstrated~~
500 ~~that PAHs can be entrapped within highly viscous, partially forming secondary organic~~
501 ~~aerosol particles during particle formation, which could cause the non-exchangeable~~
502 ~~SVOCs within particles. However, the presence and influence of the non-exchangeable~~
503 ~~SVOCs within particles on the G/P partitioning behavior were not conclusively~~
504 ~~demonstrated until now. Therefore, it is imperative to conduct studies for other~~
505 ~~influencing factors on the G/P partitioning behavior of SVOCs in future. If the influence~~
506 ~~of the total gaseous degradation and the non-exchangeable SVOCs within particles on~~
507 ~~G/P partitioning were all considered, the comprehensive understanding of the~~
508 ~~influencing factors on the deviation of K_p' from the equilibrium state might be clarified.~~

509 **5. Limitation**

510 ~~In this study, the gaseous degradation was speculated as the reason for the~~
511 ~~difference of K_p' for Me-Naps between the daytime and nighttime, which might result~~
512 ~~in the deviation of K_p' from equilibrium state for LMW SVOCs. In addition, the new~~
513 ~~steady state G-P partitioning model was used, which demonstrated that the gaseous~~
514 ~~degradation could deviate the K_p' from equilibrium state. However, there were some~~
515 ~~limitations in this study. Firstly, the different breakthrough values might occur between~~
516 ~~the daytime and nighttime, considering their different temperature. The influence of the~~
517 ~~breakthrough on K_p' was calculated, that could result into 1.20 to 1.27 times higher for~~
518 ~~K_p' in the daytime than in the nighttime, if the breakthrough (17% to 21%) only occurred~~
519 ~~in the daytime, not in the nighttime. However, the increasing of K_p' caused by the~~
520 ~~breakthrough cannot fully explain the observed diurnal variation with K_p' between~~

521 daytime and nighttime in this study (2.95 to 4.65 times). Secondly, the present study
522 only considered the gaseous degradation related to the reaction with hydroxyl radicals.
523 However, the gaseous degradation routes, like the other atmospheric oxidation
524 pathways and photodegradation were not included, which may lead to an
525 underestimation of the impact of the total gaseous degradation. Thirdly, the previous
526 studies have demonstrated that PAHs can be entrapped within highly viscous, partially
527 forming secondary organic aerosol particles during particle formation (Zelenyuk et al.,
528 2012; Shrivastava et al., 2017), which could cause the non-exchangeable SVOCs within
529 particles. However, the presence and influence of the non-exchangeable SVOCs within
530 particles on the G–P partitioning behavior were not considered in this study. Therefore,
531 it is imperative to conduct studies for other influencing factors on the G–P partitioning
532 behavior of SVOCs in future, such as the total gaseous degradation, the non-
533 exchangeable SVOCs within particles, and the advection of air masses, among others.

535 **Acknowledgments**

536 This study was supported by the National Natural Science Foundation of China (Nos.
537 42077341 and 42377377). This study was partially supported by the Heilongjiang
538 Touyan Innovation Team Program, China and High-Level Talent Funding Project of
539 Hebei Province, China~~the Postdoctoral Scientific Research Projects Funds of Hebei~~
540 ~~Province, China~~ (B2023003020).

542 **Author contributions**

543 Fu-Jie Zhu: Conceptualization, Methodology, Investigation, Writing – original draft.
544 Zi-Feng Zhang: Writing – review & editing. Li- Yan Liu: Writing – review & editing.
545 Pu-Fei Yang: Writing – review & editing. Peng-Tuan Hu: Writing – review & editing.

546 Geng-Bo Ren: Writing – review & editing. Meng Qin: Writing – review & editing.

547 Wan-Li Ma: Conceptualization, Methodology, Writing – review & editing.

548

549 **Appendix A. Supplementary data**

550 Supplementary data for this article can be found at

551

552 **References**

- 553 Baskaran, S., Lei, Y. D., and Wania, F.: Reliable prediction of the octanol-air partition ratio,
554 Environmental Toxicology and Chemistry, <https://doi.org/10.1002/etc.5201>, 2021.
- 555 Cao, R., Zhang, H., Geng, N., Fu, Q., Teng, M., Zou, L., Gao, Y., and Chen, J.: Diurnal
556 variations of atmospheric polycyclic aromatic hydrocarbons (pahs) during three sequent
557 winter haze episodes in beijing, china, Science of the Total Environment, 625, 1486-1493,
558 <https://doi.org/10.1016/j.scitotenv.2017.12.335>, 2018.
- 559 Dachs, J. and Eisenreich, S. J.: Adsorption onto aerosol soot carbon dominates gas-particle
560 partitioning of polycyclic aromatic hydrocarbons, Environmental Science & Technology,
561 34, 3690-3697, <https://doi.org/10.1021/es991201>, 2000.
- 562 Harner, T. and Bidleman, T. F.: Octanol-air partition coefficient for describing particle/gas
563 partitioning of aromatic compounds in urban air, Environmental Science & Technology,
564 32, 1494-1502, <https://doi.org/10.1021/es970890r>, 1998.
- 565 Hart, K. M. and Pankow, J. F.: High-volume air sampler for particle and gas sampling .2. Use
566 of backup filters to correct for the adsorption of gas-phase polycyclic aromatic-
567 hydrocarbons to the front filter, Environmental Science & Technology, 28, 655-661,
568 <https://doi.org/10.1021/es00053a019>, 1994.
- 569 Hart, K. M., Isabelle, L. M., and Pankow, J. F.: High-volume air sampler for particle and gas
570 sampling. 1. Design and gas sampling performance, Environmental Science & Technology,
571 26, 1048-1052, <https://doi.org/10.1021/es00029a027>, 1992.
- 572 Hu, P.-T., Ma, W.-L., Zhang, Z.-F., Liu, L.-Y., Song, W.-W., Cao, Z.-G., Macdonald, R. W.,
573 Nikolaev, A., Li, L., and Li, Y.-F.: Approach to predicting the size-dependent inhalation
574 intake of particulate novel brominated flame retardants, Environmental Science &
575 Technology, 55, 15236-15245, <https://doi.org/10.1021/acs.est.1c03749>, 2021.
- 576 Hu, P.-T., Su, P.-H., Ma, W.-L., Zhang, Z.-F., Liu, L.-Y., Song, W.-W., Qiao, L.-N., Tian, C.-
577 G., Macdonald, R. W., Nikolaev, A., Cao, Z.-G., and Li, Y.-F.: New equation to predict
578 size-resolved gas-particle partitioning quotients for polybrominated diphenyl ethers,
579 Journal of Hazardous Materials, 400, 123245,
580 <https://doi.org/10.1016/j.jhazmat.2020.123245>, 2020.
- 581 Li, Y., Ma, W., and Yang, M.: Prediction of gas/particle partitioning of polybrominated
582 diphenyl ethers (pbdes) in global air: A theoretical study, Atmospheric Chemistry and
583 Physics, 15, 1669-1681, <https://doi.org/10.5194/acp-15-1669-2015>, 2015.
- 584 Li, Y., Qiao, L., Ren, N., Sverko, E., Mackay, D., and Macdonald, R. W.: Decabrominated
585 diphenyl ethers (bde-209) in chinese and global air: Levels, gas/particle partitioning, and
586 long-range transport: Is long-range transport of bde-209 really governed by the movement
587 of particles?, Environmental Science & Technology, 51, 1035-1042,
588 <https://doi.org/10.1021/acs.est.6b05395>, 2017.
- 589 Li, Y.-F., Qiao, L.-N., Ren, N.-Q., Macdonald, R. W., and Kannan, K.: Gas/particle partitioning
590 of semi-volatile organic compounds in the atmosphere: Transition from unsteady to steady
591 state, Science of The Total Environment, 710, 136394,
592 <https://doi.org/10.1016/j.scitotenv.2019.136394>, 2020.
- 593 Li, Y. F. and Jia, H. L.: Prediction of gas/particle partition quotients of polybrominated diphenyl
594 ethers (pbdes) in north temperate zone air: An empirical approach, Ecotoxicology &
595 Environmental Safety, 108, 65-71, <https://doi.org/10.1016/j.ecoenv.2014.05.028>, 2014.
- 596 Ma, W., Zhu, F., Hu, P., Qiao, L., and Li, Y.: Gas/particle partitioning of pahs based on
597 equilibrium-state model and steady-state model, Science of The Total Environment, 706,
598 136029, <https://doi.org/10.1016/j.scitotenv.2019.136029>, 2020.
- 599 Ma, W.-L., Zhu, F.-J., Liu, L.-Y., Jia, H.-L., Yang, M., and Li, Y.-F.: Pahs in chinese
600 atmosphere: Gas/particle partitioning, Science of The Total Environment, 693, 133623,
601 <https://doi.org/10.1016/j.scitotenv.2019.133623>, 2019.
- 602 Mackay, D., Celsie, A. K. D., and Parnis, J. M.: Kinetic delay in partitioning and parallel
603 particle pathways: Underappreciated aspects of environmental transport, Environmental
604 Science & Technology, 53, 234-241, <https://doi.org/10.1021/acs.est.8b04514>, 2019.

605 Ohura, T., Horii, Y., Kojima, M., and Kamiya, Y.: Diurnal variability of chlorinated polycyclic
606 aromatic hydrocarbons in urban air, Japan, *Atmospheric Environment*, 47, 84-91,
607 <https://doi.org/10.1016/j.atmosenv.2013.08.044>, 2013.

608 Qiao, L., Hu, P., Macdonald, R., Kannan, K., Nikolaev, A., and Li, Y.: Modeling gas/particle
609 partitioning of polybrominated diphenyl ethers (pbdes) in the atmosphere: A review,
610 *Science of the Total Environment*, 729, 138962,
611 <https://doi.org/10.1016/j.scitotenv.2020.138962>, 2020.

612 Reisen, F. and Arey, J.: Atmospheric reactions influence seasonal pah and nitro-pah
613 concentrations in the Los Angeles basin, *Environmental Science & Technology*, 39, 64-73,
614 <https://doi.org/10.1021/es035454i>, 2005.

615 Sadiki, M. and Poissant, L.: Atmospheric concentrations and gas-particle partitions of
616 pesticides: Comparisons between measured and gas-particle partitioning models from
617 source and receptor sites, *Atmospheric Environment*, 42, 8288-8299,
618 <https://doi.org/10.1016/j.atmosenv.2008.07.041>, 2008.

619 Shahpoury, P., Lammel, G., Albinet, A., Sofuoglu, A., Dumanoglu, Y., Sofuoglu, S. C., Wagner,
620 Z., and Zdimal, V.: Evaluation of a conceptual model for gas-particle partitioning of
621 polycyclic aromatic hydrocarbons using polyparameter linear free energy relationships,
622 *Environmental Science & Technology*, 50, 12312-12319,
623 <https://doi.org/10.1021/acs.est.6b02158>, 2016.

624 Shrivastava, M., Lou, S., Zelenyuk, A., Easter, R. C., Corley, R. A., Thrall, B. D., Rasch, P. J.,
625 Fast, J. D., Simonich, S. L. M., Shen, H. Z., and Tao, S.: Global long-range transport and
626 lung cancer risk from polycyclic aromatic hydrocarbons shielded by coatings of organic
627 aerosol, *Proceedings of the National Academy of Sciences of the United States of America*,
628 114, 1246-1251, <https://doi.org/10.1073/pnas.1618475114>, 2017.

629 Ulrich, N., Endo, S., Brown, T. N., Watanabe, N., Bronner, G., Abraham, M. H., and Goss, K.-
630 U.: Ufz-lser database v 3.2.1 [internet], Leipzig, Germany, Helmholtz Centre for
631 Environmental Research-Ufz, 2017.

632 Wang, W., Simonich, S. L. M., Wang, W., Giri, B., Zhao, J., Xue, M., Cao, J., Lu, X., and Tao,
633 S.: Atmospheric polycyclic aromatic hydrocarbon concentrations and gas/particle
634 partitioning at background, rural village and urban sites in the North China Plain,
635 *Atmospheric Research*, 99, 197-206, <https://doi.org/10.1016/j.atmosres.2010.10.002>,
636 2011.

637 Wania, F. and Dugani, C. B.: Assessing the long-range transport potential of polybrominated
638 diphenyl ethers: A comparison of four multimedia models, *Environmental Toxicology and
639 Chemistry*, 22, 1252-1261, <https://doi.org/10.1002/etc.5620220610>, 2003.

640 Wilson, J., Pöschl, U., Shiraiwa, M., and Berkemeier, T.: Non-equilibrium interplay between
641 gas-particle partitioning and multiphase chemical reactions of semi-volatile compounds:
642 Mechanistic insights and practical implications for atmospheric modeling of PAHs,
643 *Atmospheric Chemistry and Physics*, 2020, 1-39, [https://doi.org/10.5194/acp-21-6175-
644 2021](https://doi.org/10.5194/acp-21-6175-2021), 2020.

645 Zelenyuk, A., Imre, D., Beránek, J., Abramson, E., Wilson, J., and Shrivastava, M.: Synergy
646 between secondary organic aerosols and long-range transport of polycyclic aromatic
647 hydrocarbons, *Environmental Science & Technology*, 46, 12459-12466,
648 <https://doi.org/10.1021/es302743z>, 2012.

649 Zhang, J., Yang, L., Mellouki, A., Chen, J., Chen, X., Gao, Y., Jiang, P., Li, Y., Yu, H., and
650 Wang, W.: Diurnal concentrations, sources, and cancer risk assessments of PM_{2.5}-bound
651 PAHs, NPAHs, and OPAHs in urban, marine and mountain environments, *Chemosphere*, 209,
652 147-155, <https://doi.org/10.1016/j.chemosphere.2018.06.054>, 2018.

653 Zhang, X. and McMurry, P. H.: Theoretical analysis of evaporative losses of adsorbed or
654 absorbed species during atmospheric aerosol sampling, *Environmental Science &
655 Technology*, 25, 456-459, <https://doi.org/10.1021/es00015a012>, 1991.

656 Zhu, F., Arina, S., Zhang, Z., Liu, L., Song, W., Cheng, Y., Liu, J., and Ma, W.: Non-
657 equilibrium influence on g/p partitioning of PAHs: Evidence from the diurnal and nocturnal
658 variation, *Chemosphere*, 294, 133722,
659 <https://doi.org/10.1016/j.chemosphere.2022.133722>, 2022.

660 Zhu, F.-J., Ma, W.-L., Hu, P.-T., Zhang, Z.-F., and Li, Y.-F.: Temporal trends of atmospheric
661 pahs: Implications for the influence of the clean air action, *Journal of Cleaner Production*,
662 296, 126494, <https://doi.org/10.1016/j.jclepro.2021.126494>, 2021a.

663 Zhu, F.-J., Ma, W.-L., Zhang, Z.-F., Yang, P.-F., Hu, P.-T., Liu, L.-Y., and Song, W.-W.:
664 Prediction of the gas/particle partitioning quotient of pahs based on ambient temperature,
665 *Science of The Total Environment*, 811, 151411,
666 <https://doi.org/10.1016/j.scitotenv.2021.151411>, 2021b.

667 Zhu, F. J., Hu, P. T., and Ma, W. L.: A new steady-state gas–particle partitioning model of
668 polycyclic aromatic hydrocarbons: Implication for the influence of the particulate
669 proportion in emissions, *Atmospheric Chemistry and Physics*, 23, 8583-8590,
670 <https://doi.org/10.5194/acp-23-8583-2023>, 2023.

671